

Spatiotemporal chaos in electroconvection of a homeotropically aligned nematic liquid crystal

Sheng-Qi Zhou and Guenter Ahlers

Department of Physics and iQCD, University of California, Santa Barbara, California 93106, USA

(Received 27 April 2006; published 19 October 2006)

We present patterns of electroconvection (EC) for the homeotropically aligned nematic liquid crystal MBBA. A voltage $V = \sqrt{2}V_0 \sin(2\pi ft)$ was applied. With increasing V_0 , the bend Freedericksz transition at V_F was followed by the onset of EC at $V_c > V_F$. We found four distinct pattern types. First, a primary supercritical Hopf bifurcation to traveling waves (TW's) of convection rolls occurred. The structure factor $S(\mathbf{k})$ of this state reflected the azimuthal anisotropy of the underlying Freedericksz state. For $f < f_L \approx 75$ Hz there was a superposition of two oblique-roll modes (pattern I). These patterns were chaotic in space and time. For larger f the patterns consisted of chaotic TW normal rolls (pattern II). Here the chaos was attributable to the motion of dislocations and domain walls between left- and right-traveling waves. A secondary bifurcation yielded pattern III; it had no dominant TW frequency but had broadband chaotic dynamics dominated by the motion of dislocations. This pattern type had been referred to by others as a “chevron pattern;” its structure factor still revealed azimuthal anisotropy. Finally, at somewhat larger $\epsilon \equiv V^2/V_c^2 - 1$ a highly disordered pattern IV with defect dynamics was found. This state had been studied before by Kai and co-workers and was referred to by them as “phase turbulence.” It had a structure factor that was (within our resolution) invariant under rotation. For patterns I, II, and III, $S(\mathbf{k})$ contained crescent-shaped peaks. The peak shape was qualitatively different from the case of planar EC where the structure factor has an elliptical cross section. We present measurements of the widths $1/\xi_k$ and $1/\xi_\theta$ in the radial (k) and the azimuthal (θ) directions. For small ϵ (patterns I and II) we found that ξ_k was consistent with the usual Ginzburg-Landau scaling $\xi_k \sim \epsilon^{-\nu_k}$ with $\nu_k \approx 1/2$. However, for ξ_θ we found $\xi_\theta \sim \epsilon^{-\nu_\theta}$ with $\nu_\theta \approx 3/4$. Presumably this anomalous scaling of ξ_θ is associated with the Goldstone mode of homeotropic EC. We also show data for the height S_0 of the structure factor that are consistent with $S_0 \sim \epsilon^\beta$ with $\beta \approx -0.5$, implying that S_0 diverges at onset. This differs from the case of domain chaos in rotating Rayleigh-Bénard convection where experiment is consistent with $\beta = 1/2$ and thus with a vanishing S_0 . The difference between the shape of the structure-factor cross section and between the exponents, for the present case, for planar EC, and for domain chaos suggests that there are different universality classes for spatiotemporal chaos.

DOI: [10.1103/PhysRevE.74.046212](https://doi.org/10.1103/PhysRevE.74.046212)

PACS number(s): 05.45.Jn, 47.52.+j, 47.20.Ky

I. INTRODUCTION

Electroconvection (EC) occurs in a thin layer of a nematic liquid crystal (NLC) confined between two electrodes [1,2]. A voltage $V = \sqrt{2}V_0 \sin(2\pi ft)$ will lead to convection when V_0 exceeds V_c [3–8]. One can distinguish between two cases. When the nematic director is aligned parallel to the electrodes, it breaks the rotational invariance that is characteristic of convection in isotropic systems, such as Rayleigh-Bénard convection [9]. However, when the director is aligned orthogonal to the confining surfaces (“homeotropic” alignment), the ground state of the system with $V_0 = 0$ retains the full rotational symmetry. For this case EC usually [10] is preceded by the Freedericksz transition [11] that occurs when V_0 reaches V_F . Above V_F the director develops an in-plane component that grows continuously as $V_0 - V_F$ increases [12]. This component singles out a particular direction in the plane of the sample and thus breaks the rotational invariance. Finally, above a critical voltage $V_c > V_F$, EC can occur. An interesting aspect of this system is the existence of a soft “Goldstone” mode [12] above V_F that arises from the degeneracy of the orientation of the Freedericksz state of the ideal sample [3,4,13–15]. This mode has a decisive influence on a state of spatiotemporal chaos that evolves above V_c .

In this paper we report on a study of patterns close to but above the onset of EC in a sample of the NLC

p-methoxybenzylidene-*p*-butylaniline (MBBA) with homeotropic alignment. Several earlier experimental investigations have reported on EC in homeotropic samples [6,16–29]. The patterns found close to but above onset depend on the drive frequency f and on the conductance (as determined by the concentration of ionic dopants) of the sample. Here we present features of the bifurcation diagram, the characteristics and the structure factor [(SF), the square of the modulus of the Fourier transform] of the patterns near onset, and the results of quantitative measurements of the corresponding correlation lengths.

For our sample we found that the bifurcation to EC was a supercritical Hopf bifurcation and the patterns near onset consisted of traveling waves (TW's). Theoretically the homeotropic case was considered so far only within the framework of the “standard model” [30] which predicts only supercritical stationary bifurcations. Hopf bifurcations are found from the “weak electrolyte model” (WEM) [31], which so far was applied only to the planar case. Nonlinear interactions between the traveling-wave modes contributing to the pattern led to irregular variations in space and time—i.e., to spatiotemporal chaos (STC). Using the standard model, the occurrence of STC in EC with homeotropic alignment had been predicted by Hertrich *et al.* [12] for stationary bifurcations. Examples of STC near a supercritical bifurcation are rare. They are particularly suitable for theoretical analysis because weakly nonlinear theories, perhaps in the

form of Ginzburg-Landau equations, should be usable. Notable additional cases are certain examples of EC in planar samples [32–34] and domain chaos (DC) [35–39] in rotating Rayleigh-Bénard convection which is the result of the Küppers-Lortz instability [40–42].

We found that the STC in the present system differs qualitatively from DC and planar EC in that the SF has different symmetry properties. Its horizontal cross sections are crescent shaped and extend along a circle about the origin. In contrast to that, the SF for DC forms an azimuthally uniform ring in Fourier space and the SF for planar EC has peaks with elliptic cross sections with a major-axis orientation that varies with f and σ [32–34,43]. In addition, the exponents describing the scaling of the azimuthal correlation length and the height of the SF with $\epsilon \equiv V_0^2/V_c^2 - 1$ for the present case have values that differ from the usual Landau values of $1/2$ characteristic of planar EC and DC [44]. The results for these systems provide experimental evidence for the idea that there exist different universality classes of STC that can be characterized for instance by the symmetry properties and characteristic exponents of their structure factors.

The rest of the paper is organized as follows. In Sec. II we present some experimental details and the image-analysis methods. In Sec. III we describe four qualitatively different patterns that were observed, discuss their general features, and show the ϵ and f ranges over which they exist. In Sec. IV we give results of the correlation-length measurements. The dependence of the height S_0 of $S(\mathbf{k})$ on ϵ is discussed in Sec. V. A summary is given in Sec. VI.

II. EXPERIMENTAL PROCEDURE AND IMAGE ANALYSIS

The apparatus was described before [28,33]. Here only key procedures are mentioned. The homeotropic cell consisted of two parallel indium-tin oxide- (ITO-) coated glass plates. The insides of these plates were spin coated with a special polyimide [45]. The sample consisted of MBBA (*p*-methoxybenzylidene-*p*-butylaniline). The conductance σ of the MBBA was adjusted by the addition of 50 ppm tetra-*n*-butyl-ammonium bromide (TBAB) which yielded $\sigma_{\parallel} = 5.6 \times 10^{-8} \Omega^{-1} \text{m}^{-1}$ parallel to the director. The sample was the same as MBBA-4 of Ref. [28]. After preparing it, it was allowed to age for 3 months. Thereafter our measurements were carried out during an additional 2 months. The total size of the sample was $19.3 \times 15.4 \text{ mm}^2$. The cell thickness was measured with an interferometer [46] and found to be $41.8 \mu\text{m}$, yielding an aspect ratio of 462×368 [47]. A much smaller area—for instance, $1.4 \times 1.4 \text{ mm}^2$ as shown in Fig. 1—was selected for detailed study. The cell was kept at $25.00 \pm 0.01 \text{ }^\circ\text{C}$ throughout the experiment.

As V_0 was increased beyond $V_F = 3.9 \text{ V}$, a transition occurred from the uniform homeotropic state to the Fredericksz state as discussed elsewhere [28]. Above V_f a single uniform domain covered the entire sample. Above V_F and at a fixed driving frequency f , we changed V_0 monotonically with nonequal steps; the steps became smaller near the estimated EC threshold. At each V_0 , we waited 1200 s and then took 128 images $\tilde{I}_i(\mathbf{x}, \epsilon)$. The time interval between images

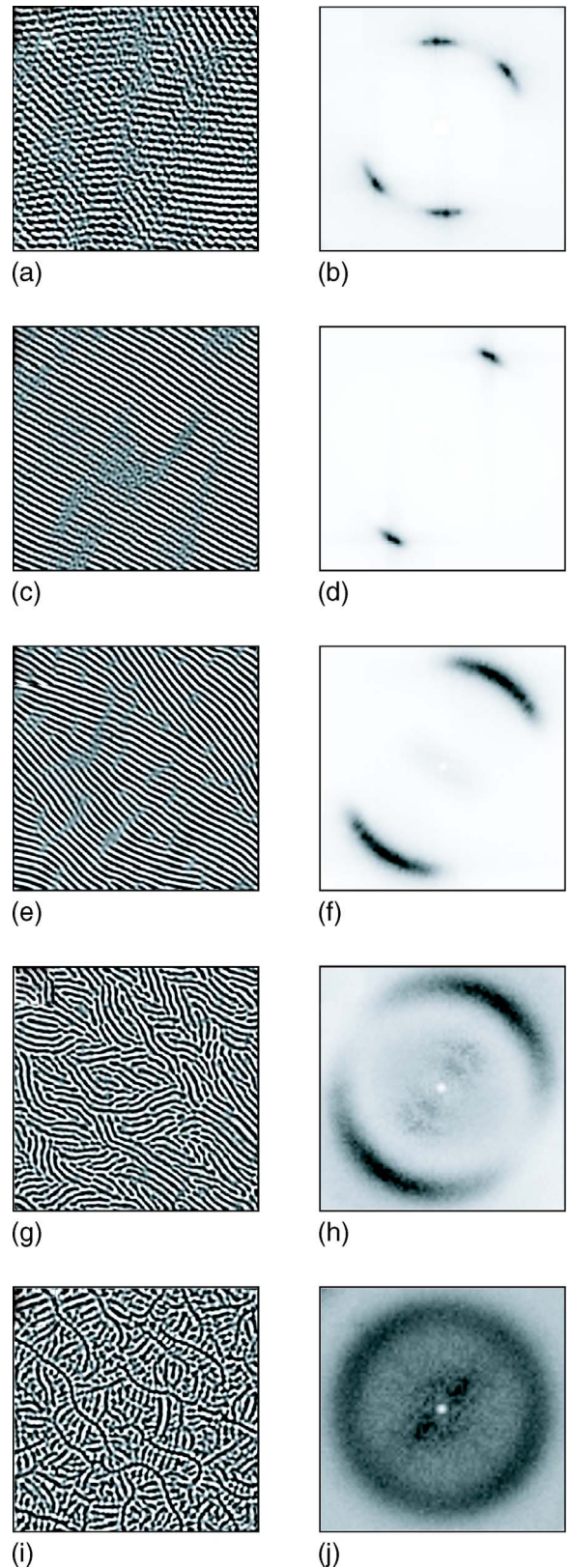


FIG. 1. (Color online) (a) is a shadowgraph image at $f=20 \text{ Hz}$ and $\epsilon=0.003$. (b) is its structure factor. (c), (e), (g), and (i) are shadowgraph images at $f=100 \text{ Hz}$ with $\epsilon=0.0029, 0.019, 0.086,$ and 0.159 , respectively. (d), (f), (h), and (j) are the corresponding structure factors. The images cover an area of $1.4 \times 1.4 \text{ mm}^2$ and the structure factors are for $-7.9 \leq (k_x, k_y) \leq 7.9$.

was 30 s, yielding nearly uncorrelated images; however, the time interval was reduced to 0.5 s for the construction of the movies to show the traveling waves. The images had a physical size of $1.4 \times 1.4 \text{ mm}^2$ and were digitalized with a spatial resolution of 420×420 pixels using 4096 gray levels.

The image-analysis method is described in detail in Ref. [48]. Briefly, each image was normalized with a background image in the form of $I_i(\mathbf{x}, \epsilon) = \tilde{I}_i(\mathbf{x}, \epsilon) / \tilde{I}_0(\mathbf{x}, \epsilon) - 1$. Here $\tilde{I}_0(\mathbf{x}, \epsilon)$ is the average of all 128 images. For each normalized image $I_i(\mathbf{x}, \epsilon)$, the structure factor $S_i(\mathbf{k}, \epsilon)$ (the square of the modulus of the Fourier transform) was calculated and 128 $S_i(\mathbf{k}, \epsilon)$ were averaged to obtain $S(\mathbf{k}, \epsilon)$. Here $\mathbf{k} = (k_x, k_y)$ is the wave vector of the pattern. Its magnitude is $k = \sqrt{k_x^2 + k_y^2}$, and its angle is $\theta = \tan^{-1}(k_y/k_x)$. Throughout this paper length is scaled by the sample spacing d .

III. QUALITATIVE FEATURES OF THE PATTERNS, THE STRUCTURE FACTORS, AND THE PHASE DIAGRAM

In a previous paper [28] the properties of our sample directly at onset were reported already [47]. Above onset we found four distinct pattern types, with different symmetries. Representative snapshots of each are shown in Figs. 1(a), 1(c), 1(e), 1(g), and 1(i), and the dynamics of these patterns is illustrated by five MPEG movies [49], with one each corresponding to the snapshots in Fig. 1.

At low frequencies a primary supercritical bifurcation [28] yielded a chaotic superposition of traveling oblique rolls [pattern I, Fig. 1(a), ZA06_Pattern_I.mpeg]. This pattern type was qualitatively similar to ones reported in Refs. [17,19,23] for EC in homeotropic samples. Superficially it was also similar to STC found with the NLC I52 and planar alignment [32,33]. However, it should be noted that it differed from the planar case in an important way. Looking at Fig. 1(b) one sees that the four peaks of its SF are crescent shaped as mentioned above, whereas the planar case has SF peaks of elliptic cross section.

As the drive frequency f was increased, the primary bifurcation changed at a Lifshitz frequency $f_L \approx 75 \text{ Hz}$ ($f\tau_q \approx 0.10$ where $\tau_q \approx 0.0013 \text{ s}$ is the charge relaxation time; see [28]) from yielding traveling oblique rolls to producing traveling normal rolls. These normal rolls contained many defects and domain walls between left- and right-traveling waves [pattern II, Figs. 1(c) and 1(e), ZA06_Pattern_Iia.mpeg and ZA06_Pattern_Iib.mpeg]. The appearance of snapshots of these patterns was similar to that reported in Refs. [17–19]. The TW frequencies of patterns I and II decreased with increasing ϵ from their Hopf value at the primary bifurcation [28], but they remained finite until a secondary bifurcation was reached.

At the secondary bifurcation pattern III was entered [Fig. 1(g), ZA06_Pattern_III.mpeg]. Pattern III did not contain a dominant traveling-wave frequency, but showed broadband chaotic dynamics associated with the motion of numerous dislocations. The extent of its disorder in the angular coordinate was greater than that of pattern II and increased with ϵ . Qualitatively similar patterns were reported in Ref. [23],

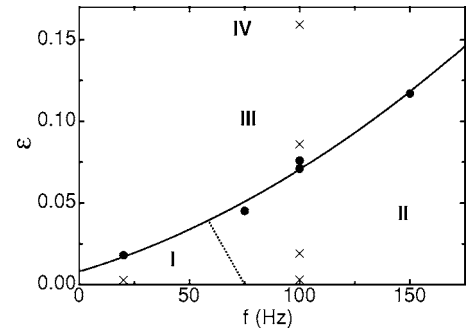


FIG. 2. The ϵ -frequency plane showing the location of the four patterns observed in this work. The points marked by \times , in the sequence from left to right and then from bottom to top, are the locations for the images in Fig. 1. The solid circles are the locations ϵ_c of transitions between different patterns as determined from the correlation lengths ξ_k ; see Fig. 3. The solid line is a fit of a quadratic equation to the circles. The dotted line is the approximate location of the Lifshitz line.

where they were referred to as “Chevron patterns.” Similar patterns were found also in Ref. [25], where they were called “defect-mediated chevron patterns.”

Finally, with increasing V_0 a highly disordered state [pattern IV, Fig. 1(i), ZA06_Pattern_IV.mpeg] evolved that was also chaotic in space and time. It also did not reveal a characteristic traveling-wave frequency. This state was studied before in some detail by Kai and co-workers [20–22]. A pattern similar to Fig. 1(i) and a corresponding structure factor similar to Fig. 1(j) are shown, for instance, in Fig. 3 of Ref. [20]. These authors referred to this pattern type as “soft-mode turbulence.” In our sample this state did not occur near onset and formed only well above the secondary bifurcation mentioned above. Within our resolution its structure factor was invariant under rotation, indicating that the vigorous chaotic dynamics was able to overcome completely the anisotropy due to the Freedericksz state.

For patterns I–III the structure factors had the shape of crescents oriented along a circle about the origin in k space. For pattern IV, $S(\mathbf{k})$ consisted of a circular band that was, within our resolution, invariant under rotation. This differs qualitatively from the structure factors of samples with planar alignment, which have an elliptic shape. Further, in the planar case the ellipses corresponding to oblique rolls generally do not have their major axes tangential to a circle drawn about the origin and through the peak [33,34]. We attribute the considerable width $1/\xi_\theta$ in the azimuthal direction to the rotational invariance of the ground state of the homeotropic system below the Freedericksz transition and to the Goldstone mode [12] that persists above the Freedericksz transition; the deviation from full rotational invariance reflects the broken symmetry due to the Freedericksz state. Quantitative measurements of the widths $1/\xi_k$ and $1/\xi_\theta$ of $S(\mathbf{k})$ in the radial and azimuthal directions, respectively, as functions of ϵ over a range of driving frequencies f will be given below in Sec. IV.

In Fig. 2 we show the regions in the ϵ - f plane where the four patterns occur. The points marked by an \times , from left to right and then from bottom to top, correspond to the pattern

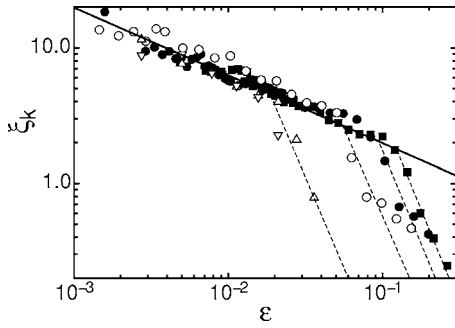


FIG. 3. The correlation length ξ_k as a function of ϵ of zig (open up-pointing triangles) and zag (open down-pointing triangles) rolls at $f=20$ Hz and of normal rolls at $f=75$ Hz (open circles), 100 Hz (solid circles), 150 Hz (solid squares). The solid line corresponds to the power law $\xi_k=0.62\epsilon^{-1/2}$. The dashed lines have slopes corresponding to effective exponents close to -2.5 and are intended to illustrate the rapid decrease of ξ_k for $\epsilon > \epsilon_c(f)$.

sequence in Fig. 1. Pattern I [Fig. 1(a)] corresponds to coexisting “zig” and “zag” oblique traveling rolls. At onset the Lifshitz point separating pattern I from pattern II occurred at $f_L \simeq 75$ Hz. The location of the dotted line between I and II is only approximate and was not determined with high resolution. However, for $f=f_L$ we found only normal rolls as ϵ was increased up to the secondary bifurcation (solid line). Thus the Lifshitz line either is vertical or tilted slightly toward the left as shown in the figure.

The solid line separating I and II from III and IV indicates the location of a secondary bifurcation and was determined from a dramatic change of the ϵ dependence of a correlation length as discussed in Sec. IV and shown below in Fig. 3. With further increase of ϵ we obtain pattern IV. We have not been able to establish unequivocally whether pattern IV comes into existence via a tertiary bifurcation or whether it evolves via a crossover associated with a continuous evolution of $S(\mathbf{k})$ from a crescent shape as shown in Fig. 1(h) to a rotationally invariant annular shape as shown in Fig. 1(j).

IV. CORRELATION LENGTHS

Here we present quantitative results for the inverse widths, or correlation lengths, of $S(\mathbf{k})$ for patterns I, II, and III. Measurements of a correlation length were made before for MBBA with homeotropic alignment, albeit for samples with the much larger conductance $\sigma_{\parallel}=2.9 \times 10^{-7} \Omega^{-1} \text{m}^{-1}$ where we expect the bifurcation to EC to be stationary [28] rather than of the Hopf type to traveling waves as in our case.

The shape of $S(\mathbf{k})$ in Fig. 1 suggests that it can be described best in polar coordinates $\mathbf{k}=(k, \theta)$ with maxima located at k_0 and θ_0 [50]. An analytic form for $S(k, \theta)$ is not known from theory and must be chosen empirically. In previous analyses of structure factors of EC with planar alignment and of Rayleigh-Bénard convection [34,44,48,51,52] both Lorentzian and Swift-Hohenberg [53,54] forms were used. It was found [44] that both give very similar values for the widths at half-height. We tried different forms for the

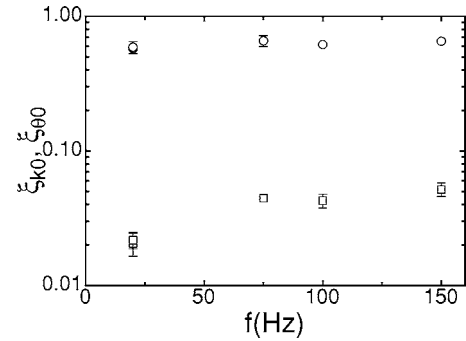


FIG. 4. The correlation-length amplitudes ξ_{k_0} (circles) and ξ_{θ_0} (squares) as a function of the driving frequency f .

two-dimensional structure factor as functions of k and θ and found that the function

$$S(k, \theta) = \frac{S_0}{\xi_k^2(k^2 - k_0^2)^2 / (4k_0^2) + k_0^2 \xi_\theta^2(\theta - \theta_0)^2 + 1} \quad (1)$$

gives a good fit to the data. It uses a Swift-Hohenberg form [53,54] in the radial (i.e., k) direction, thus assuring a finite total power. A Lorentzian form is used in the azimuthal direction, but a SH form gave nearly as good a fit to the data. For $k=k_0$ it is easy to see that the half-width at half-height in the azimuthal direction is equal to $1/(k_0 \xi_\theta)$. Least-squares fits of Eq. (1) to the data for $S(k, \theta)$ at each ϵ yielded $S_0(\epsilon)$, $\xi_k(\epsilon)$, and $\xi_\theta(\epsilon)$.

Figure 3 shows the results of ξ_k as a function of ϵ for different driving frequencies. For sufficiently small ϵ the data can be represented well by a power law, with an exponent $\nu_k=1/2$ as predicted by Ginzburg-Landau-like models and as shown by the solid line in the figure.

One of the significant features of ξ_k is that it reveals a transition at a well-defined value $\epsilon=\epsilon_c$. This transition corresponds to a change from patterns of type I or II to type III. It also corresponds to the point of disappearance of the traveling waves; i.e., beyond it there was no dominant frequency and the pattern dynamics was dominated by dislocation motion and yielded only a broad spectrum. Below this transition, a fit of a powerlaw $\xi_k=\xi_{k_0}\epsilon^{-\nu_k}$ to the data yielded $\nu_k=0.51, 0.54, 0.52, 0.43,$ and 0.55 for the zig and zag modes at $f=20$ Hz and for the normal rolls at $f=75, 100, 150$ Hz, respectively. These results are in very good agreement with the value $\nu=1/2$ that follows from all Ginzburg-Landau-type models that contain terms linear in ϵ and second-order gradient terms. When ν_k was fixed at $1/2$, ξ_{k_0} was found to be constant within experimental uncertainty and equal to 0.62 ± 0.05 as shown by the open circles in Fig. 4. We fitted all measurements of ξ_k below $\epsilon_c(f)$ together with ν fixed at $1/2$. It gave $\xi_{k_0}=0.626$ and the solid line in Fig. 3.

Results for ξ_θ are shown in Fig. 5. These data have somewhat more scatter than those for ξ_k , but within their resolution seem to vary smoothly through ϵ_c . The values of ξ_θ are generally smaller than those for ξ_k , indicating the greater width of $S(\mathbf{k})$ in the azimuthal direction [55]. The data were fitted by the power law $\xi_\theta=\xi_{\theta_0}\epsilon^{-\nu_\theta}$ and gave $\nu_\theta=0.77, 0.87, 0.75, 0.75,$ and 0.84 for zig and zag modes at $f=20$ Hz and

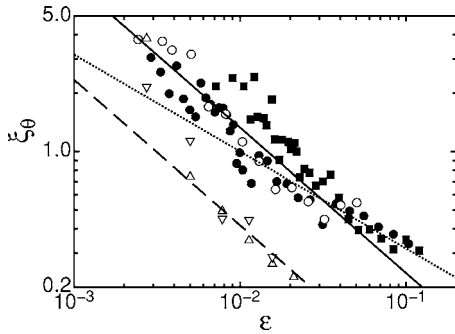


FIG. 5. The correlation length ξ_θ as a function of ϵ of zig (open up-pointing triangles) and zag (open down-pointing triangles) rolls at $f=20$ Hz and of normal rolls at $f=75$ Hz (open circles), 100 Hz (solid circles), 150 Hz (solid squares). The solid line is the power law $\xi_\theta=0.042\epsilon^{-3/4}$. The dashed line corresponds to $\xi_\theta=0.013\epsilon^{-3/4}$. The dotted line has a slope of $-1/2$.

for the normal rolls at $f=75, 100, 150$ Hz, respectively. These values are close to $3/4$ and definitively larger than the usual Ginzburg-Landau value of $1/2$. We presume that the large value of ν_θ is associated with the Goldstone mode of this system, but are not aware of a specific theoretical prediction. When ν_θ was fixed at $3/4$, a fit of all the data for $f > f_L$ yielded the solid line in Fig. 5 with the amplitude $\xi_{\theta 0}=0.042$. Separate fits for each f with $\nu_\theta=3/4$ gave the amplitudes $\xi_{\theta 0}$ shown as open squares in Fig. 4. It is noticeable that the $\xi_{\theta 0}$ values in the normal-roll regime above the Lifshitz point ($f=75, 100, 150$ Hz) are nearly independent of f and close to 0.044 . In the oblique-roll regime at $f=20$ Hz the amplitude is smaller by about a factor of 2.

In recent work on domain chaos it was found that Fourier analysis yields correlation lengths that are image-size dependent [44]. To rule out finite image-size effects in the present work, we analyzed images of two different sizes for $f=100$ Hz: namely, 1.4×1.4 mm² and 0.84×0.84 mm². In Fig. 6 results from the larger (smaller) image size are shown as solid symbols (open symbols). For ξ_k (circles) as well as for ξ_θ (squares) one sees that both images sizes agree with each other within the experimental resolution. Thus we believe that the finite image-size effect does not play an important role for the present work.

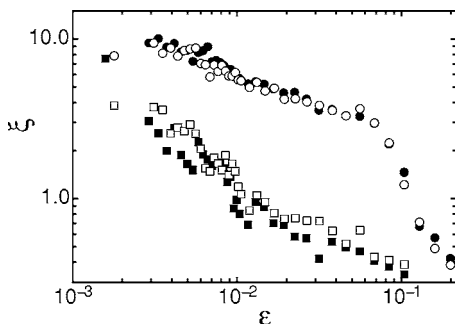


FIG. 6. The correlation lengths ξ_k (circles) and ξ_θ (squares) at $f=100$ Hz. The images cover an area of 1.4×1.4 mm² for solid symbols and an area of 0.84×0.84 mm² for open symbols.

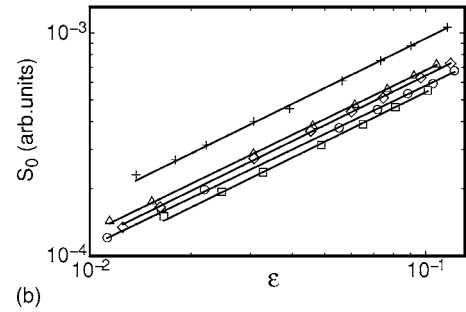
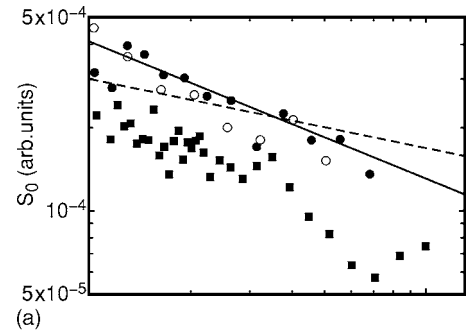


FIG. 7. (a) The amplitude S_0 [see Eq. (1)] of the structure factor as a function of ϵ for normal rolls at $f=75$ Hz (open circles), 100 Hz (solid circles), and 150 Hz (solid squares). The power law $S_0 \sim \epsilon^{-1/2}$ ($S_0 \sim \epsilon^{-1/4}$) is shown as a solid (dashed) line. (b) The amplitude S_0 of the structure factor for domain chaos as given in Fig. 20 of Ref. [44] for several rotation rates Ω .

V. HEIGHT S_0 OF $S(\mathbf{k})$

A further potentially singular parameter in Eq. (1) is its height S_0 . It is displayed in Fig. 7(a). Although the data show considerable scatter especially at the larger V_0 , S_0 can be described reasonably well by a power law $S_0 \sim \epsilon^\beta$. The results indicate that $\beta < 0$ and are consistent with $\beta = -1/2$ as shown by the solid line. This implies that S_0 diverges as $\epsilon \rightarrow 0$.

It is interesting to compare the above result with the equivalent parameter for domain chaos. The results from Fig. 20 of Ref. [44] are reproduced for comparison in Fig. 7(b). They are described quite well by a power law with $\beta_{KL} = 1/2$; i.e., S_0 vanishes as $\epsilon \rightarrow 0$.

The integral of $S(\mathbf{k})$ is equal to the total power $P(\epsilon)$, which in turn by virtue of Parseval's theorem equals the variance of the image in real space. One would expect $P(\epsilon) \sim \epsilon^\pi$ with $\pi=1$ as $\epsilon \rightarrow 0$. For several functional forms of $S(\mathbf{k})$, $P(\epsilon)$ is proportional to the cross-sectional area at half height times S_0 [44]. Assuming that this is the case here as well, we expect the scaling law $\pi = \beta + \nu_k + \nu_\theta$ to hold. Using $\pi=1$, $\nu_k=1/2$, and $\nu_\theta=3/4$, one then has $\beta = -1/4$ rather than $-1/2$ as suggested by the solid line in Fig. 7. A power law with $\beta = -1/4$ is shown by the dashed line in the figure. It does not seem to be consistent with the data, but more quantitative measurements would be helpful.

VI. SUMMARY

In this paper we presented shadowgraph images of patterns of electroconvection in a homeotropically aligned

nematic liquid crystal. We found four pattern types. These are illustrated in Fig. 1 as well as by five MPEG movies [49]. Immediately above onset a supercritical Hopf bifurcation yielded oblique TW's (pattern I) at low and normal TW's (pattern II) at high drive frequencies. The Lifshitz frequency that separates the two regions was near $f_L=75$ Hz. The oblique-roll state consisted of a chaotic superposition of left and right TW's of each of the two oblique-roll modes. The normal TW above f_L consisted of coexisting domains of left- and right-traveling waves separated spatially by domain walls and dislocations that had a chaotic temporal and spatial dependence. We note that these patterns differ qualitatively from the chaotic state referred to as "soft mode turbulence" in Ref. [20]. Although we do not know the reason for this difference, we mention that the conductance σ_{\parallel} of their sample was $3.3 \times 10^{-7} \Omega^{-1} \text{ m}^{-1}$ where the primary bifurcation to EC is stationary, whereas we found a Hopf bifurcation for our sample with $\sigma_{\parallel}=5.6 \times 10^{-8} \Omega^{-1} \text{ m}^{-1}$.

A secondary bifurcation from either pattern I or II yielded a new state (pattern III) without a characteristic frequency but with broadband dynamics in the form of the motion of many dislocations. This state had been reported before in Ref. [23] where it was referred to as "Chevron patterns" and in Ref. [25] where it was called "defect-mediated chevron (DMC) patterns." Finally, further above onset the pattern was even more disordered (pattern IV) and assumed the characteristics of the state referred to as "soft mode turbulence" by Kai and co-workers [20–22]. We were unable so far to determine whether pattern IV evolved continuously from pattern III or whether it was achieved via a tertiary bifurcation.

An interesting characteristic of all the patterns is that their structure factor (SF) has a crescent shape, with peaks that extend azimuthally in k space. This symmetry differs from

that of the SF of domain chaos in rotating Rayleigh-Benard convection [44] where the SF consist of a uniform annulus in Fourier space and from that of planar electroconvection where the SF peaks have an elliptic cross section.

Close to onset the SF for our samples can be characterized by a maximum height $S_0 \sim \epsilon^\beta$ and by two correlation lengths $\xi_k \sim \epsilon^{-\nu_k}$ and $\xi_\theta \sim \epsilon^{-\nu_\theta}$ equal to the inverse half widths of the SF peak in the radial (k) and azimuthal (θ) directions, respectively. We find that the measurements of ξ_k are consistent with the usual Ginzburg-Landau (GL) scaling $\nu_k=1/2$. On the other hand, we find that $\nu_\theta \approx 3/4$. This differs from the GL prediction and from other cases known from experiment. We conjecture that this anomaly is associated with the Goldstone mode that is predicted [12] for this system.

As was shown analytically for certain empirical functions used to fit $S(\mathbf{k})$ [44], it seems reasonable to assume that the total power $P \sim \epsilon^\pi$ is proportional to the cross-sectional area $1/(\xi_k \xi_\theta)$ times the height S_0 of the SF. This yields the scaling law $\pi = \beta + \nu_k + \nu_\theta$. Assuming that the total power vanishes linearly as $\epsilon \rightarrow 0$ (i.e., $\pi=1$), one expects $\beta = -1/4$ for our experimental values of ν_k and ν_θ . Although the data for S_0 have considerable scatter, they suggest that β is closer to $-1/2$, but further measurements are needed to clarify this point.

The qualitative difference between the shapes of the SF for our homeotropic case, for EC with planar alignment, and for domain chaos suggests that one can define different universality classes for spatiotemporal chaos on the basis of these symmetries and the corresponding exponents.

ACKNOWLEDGMENT

This work was supported by the U.S. National Science Foundation through Grant No. DMR02-43336.

-
- [1] See, for instance, L. M. Blinov, *Electro-Optical and Magneto-Optical Properties of Liquid Crystals* (Wiley, New York, 1983).
- [2] See, for instance, P. G. de Gennes and J. Prost, *The Physics of Liquid Crystals* (Clarendon Press, Oxford, 1993).
- [3] L. Kramer and W. Pesch, *Annu. Rev. Fluid Mech.* **27**, 515 (1995).
- [4] L. Kramer and W. Pesch, in *Pattern Formation in Liquid Crystals*, edited by A. Buka and L. Kramer (Springer-Verlag, Berlin, 1996).
- [5] W. Pesch and U. Behn, in *Evolution of Spontaneous Structures in Dissipative Systems*, edited by F. H. Busse and S. C. Mueller (Springer, Berlin, 1998).
- [6] Á. Buka, P. Tóth, N. Éber, and L. Kramer, *Phys. Rep.* **337**, 157 (2000).
- [7] L. Kramer and W. Pesch, in *Physical Properties of Nematic Liquid Crystals*, edited by D. A. Dummur, A. Fukuda, and G. R. Luckhurst, *Emis Datareview Series No. 25* (INSPEC, London, 2001).
- [8] For a recent review of the dependence of EC on the director-orientation geometry and on the material parameters, see Á. Buka, N. Éber, W. Pesch, and L. Kramer, in *Self-Assembly, Pattern Formation, and Growth Phenomena in Nano-Systems*, edited by A. A. Golovin and A. A. Nepomnyashchy, Vol. 218 of *NATO Science Series II: Mathematics, Physics, and Chemistry* (Springer, Dordrecht, 2006), pp. 55–82.
- [9] For a review, see, for instance, E. Bodenschatz, W. Pesch, and G. Ahlers, *Annu. Rev. Fluid Mech.* **32**, 709 (2000).
- [10] See, however, Á. Buka, B. Dressel, L. Kramer, and W. Pesch, *Phys. Rev. Lett.* **93**, 044502 (2004).
- [11] V. Fréedericksz and V. Zolina, *Trans. Faraday Soc.* **29**, 919 (1933).
- [12] A. Hertrich, W. Decker, W. Pesch, and L. Kramer, *J. Phys. II* **2**, 1915 (1992).
- [13] A. G. Rossberg, A. Hertrich, L. Kramer, and W. Pesch, *Phys. Rev. Lett.* **76**, 4729 (1996).
- [14] A. G. Rossberg and L. Kramer, *Phys. Scr.* **T67**, 121 (1996).
- [15] A. G. Rossberg, N. Éber, Á. Buka, and L. Kramer, *Phys. Rev. E* **61**, R25 (2000).
- [16] S. Kai and W. Zimmermann, *Prog. Theor. Phys. Suppl.* **99**, 458 (1989).
- [17] H. Richter, N. Klöpper, A. Hertrich, and A. Buka, *Europhys. Lett.* **30**, 37 (1995).
- [18] H. Richter, Á. Buka, I. Rehberg, and P. Cladis, in *Spatio-*

- Temporal Patterns in Nonequilibrium Complex Systems*, edited by P. E. Cladis and P. P. Palfy-Muhoray (Addison-Wesley, Reading, MA, 1995), p. 343.
- [19] H. Richter, Á. Buka, and I. Rehberg, *Phys. Rev. E* **51**, 5886 (1995).
- [20] S. Kai, K-i Hayashi, and Y. Hidaka, *J. Phys. Chem.* **100**, 19007 (1996).
- [21] Y. Hidaka, J.-H. Huh, K. I. Hayashi, S. Kai, and M. I. Tribelsky, *Phys. Rev. E* **56**, R6256 (1997).
- [22] Y. Hidaka, J.-H. Huh, K.-i. Hayashi, M. I. Tribelsky, and S. Kai, *J. Phys. Soc. Jpn.* **66**, 3329 (1997).
- [23] P. Tóth, Á. Buka, J. Peinke, and L. Kramer, *Phys. Rev. E* **58**, 1983 (1998).
- [24] N. Éber, A. G. Rossberg, Á. Buka, and L. Kramer, *Mol. Cryst. Liq. Cryst. Sci. Technol., Sect. A* **351**, 161 (2000).
- [25] J.-H. Huh, Y. Hidaka, A. G. Rossberg, and S. Kai, *Phys. Rev. E* **61**, 2769 (2000).
- [26] K. Tamura, Y. Yusuf, Y. Hidaka, and S. Kai, *J. Phys. Soc. Jpn.* **70**, 2805 (2001).
- [27] K. Tamura, Y. Hidaka, Y. Yusuf, and S. Kai, *Physica A* **306**, 157 (2002).
- [28] S.-Q. Zhou, N. Éber, Á. Buka, W. Pesch, and G. Ahlers, *Phys. Rev. E* , (2006) (preceding paper).
- [29] Several investigations of this system in the presence of a magnetic field in the plane of the sample have been carried out as well. In the present paper we do not address the influence of such a field.
- [30] E. Bodenschatz, W. Zimmermann, and L. Kramer, *J. Phys. (Paris)* **49**, 1875 (1988), and references therein.
- [31] M. Treiber and L. Kramer, *Phys. Rev. E* **58**, 1973 (1998), and references therein.
- [32] M. Dennin, G. Ahlers, and D. S. Cannell, *Science* **272**, 388 (1996).
- [33] M. Dennin, D. S. Cannell, and G. Ahlers, *Phys. Rev. E* **57**, 638 (1998).
- [34] M. A. Scherer and G. Ahlers, *Phys. Rev. E* **65**, 051101 (2002).
- [35] K. E. Heikes and F. H. Busse, *Ann. N.Y. Acad. Sci.* **357**, 28 (1980).
- [36] F. H. Busse and K. E. Heikes, *Science* **208**, 173 (1980).
- [37] Y. Hu, R. E. Ecke, and G. Ahlers, *Phys. Rev. Lett.* **74**, 5040 (1995).
- [38] Y. Hu, R. E. Ecke, and G. Ahlers, *Phys. Rev. E* **55**, 6928 (1997).
- [39] Y. Hu, W. Pesch, G. Ahlers, and R. E. Ecke, *Phys. Rev. E* **58**, 5821 (1998).
- [40] G. Küppers and D. Lortz, *J. Fluid Mech.* **35**, 609 (1969).
- [41] G. Küppers, *Phys. Lett.* **32A**, 7 (1970).
- [42] R. M. Clever and F. H. Busse, *J. Fluid Mech.* **94**, 609 (1979).
- [43] X. Xu, Ph.D. thesis, University of California at Santa Barbara, 2005.
- [44] N. Becker and G. Ahlers, *Phys. Rev. E* **73**, 046209 (2006).
- [45] Model SE-1211 in Nissan Chemical America Corporation, Houston, TX, USA.
- [46] J. R. deBruyn, E. Bodenschatz, S. Morris, S. Trainoff, Y.-C. Hu, D. S. Cannell, and G. Ahlers, *Rev. Sci. Instrum.* **67**, 2043 (1996).
- [47] The present sample is sample MBBA-4 of Ref. [28].
- [48] U. Bisang and G. Ahlers, *Phys. Rev. E* **60**, 3910 (1999).
- [49] See EPAPS Document No. E-PLLEE8-74-031610 for five MPEG movies corresponding to the snapshots in Figs. 1(a), 1(c), 1(e), 1(g), and 1(i). This document can be reached via a direct link in the online article's HTML reference section or via the EPAPS homepage (<http://www.aip.org/pubservs/epaps.html>). The movies cover smaller areas ($1.21 \times 1.21 \text{ mm}^2$) than the snapshots in Fig. 1. When played at 30 frames per second, they run at $5 \times$ actual speed.
- [50] As discussed in a previous publication [28], θ_0 does not coincide precisely with the orientation of the Fredericksz state.
- [51] X. L. Qiu and G. Ahlers, *Phys. Rev. Lett.* **94**, 087802 (2005).
- [52] J. M. Ortiz de Zárate and J. V. Sengers, *Phys. Rev. E* **66**, 036305 (2002).
- [53] J. B. Swift and P. C. Hohenberg, *Phys. Rev. A* **15**, 319 (1977).
- [54] P. C. Hohenberg and J. B. Swift, *Phys. Rev. A* **46**, 4773 (1992).
- [55] Because ξ_θ is the inverse half width of the structure factor in the azimuthal direction, it has a lower bound corresponding to the rotationally invariant SF found at large ϵ . Fitting data for pattern type IV we found $\xi_\theta \approx 0.05$, a factor of 3 smaller than any of the values shown in Fig. 5.